International Symposium
On Turbulence and Shear Flow
Phenomena (TSFP-9)
June 30 - July 3, 2015 *Melbourne, Australia*

SHEARLESS MIXING LAYER IN GRID GENERATED TURBULENCE AT MODERATE REYNOLDS NUMBER

Md Kamruzzaman[†], **L. Djenidi and R. A. Antonia**
School of Engineering
University of Newcastle
University drive, Callaghan, NSW 2308, Australia
[†]Md.Kamruzzaman@uon.edu.au

ABSTRACT

The decay of turbulence in a shearless mixing layer generated from the junction of side by side grids with different mesh sizes but identical solidity is being investigated using hot wire anemometry. It is observed that turbulence decays according to a power-law, albeit, with a different power-law exponent (n) for each grid. The measurements suggest the existence of turbulent energy transfer from the larger mesh region to the smaller mesh region at distances as large as 75 M_L from the grid, where M_L is the mesh size of the larger mesh grid. It is further observed that the Reynolds number R_λ remains constant along the centreline of the flow (*i.e.* the junction of the two grids), confirming that self-preservation is satisfied in this region of the flow. This is supported by the one dimensional velocity spectra $E_u(k_1)$. On the centreline, the measured energy spectra at positions $x/M_L \geq 45$ collapse onto a single curve at all wavenumbers when scaled by either the Kolmogorov velocity and length scales or the *rms* velocity (u') and Taylor microscale (λ). Away from the centreline the spectra do not present such collapse.

INTRODUCTION

The study of a shearless mixing layer (hereafter, SML) is of fundamental importance in understanding a variety of laboratory and geophysical flows. Several investigations have been carried out in the past to understand the interaction between two different energy containing regions in a SML, (see, for example, Gilbert (1980); Veeravalli & Warhaft (1989); Briggs *et al.* (1996); Knaepen & Carati (2004); Tordella & Iovieno (2006) and Kang & Meneveau (2008)). Gilbert (1980) conducted the first experimental investigation on a SML by using a passive grid with a zero mean velocity gradient in the lateral direction. He mainly studied the downstream evolution of the mixing layer and mixing associated with the turbulent kinetic energy diffusion. Later, Veeravalli & Warhaft (1989)(hereafter, V&W) studied the shearless mixing layer by using two different grids (*e.g.* parallel bar grid and perforated grid). They observed that the mixing layer is strongly intermittent with non-Gaussian velocity distributions as the high intensity turbulence is transported to the lower intensity region. Recently, Briggs *et al.* (1996) and Tordella & Iovieno (2006) performed numerical simulations on the interaction between different decaying homogeneous and isotropic turbulence and offered more information on the Gaussian asymptotic state in the absence of mean velocity gradient. Most of these studies were conducted in the regions close to the grid ($x/M \leq 36$), except Tordella & Iovieno (2006).

Here, we investigate the SML in the region $45 \leq x/M_L \leq 75$, which is well beyond the region so far explored as reported in the literature. The main purpose of the present work is to assess how the turbulence in a SML decays, in particular, whether self-preservation (hereafter denoted SP) can be attained within this flow region downstream of the grid.

EXPERIMENTS AND MEASUREMENT TECHNIQUES

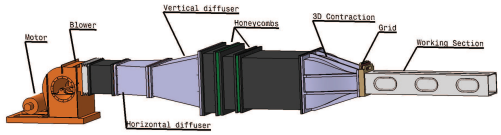

Figure 1. A three-dimensional sketch of the wind tunnel.

The wind tunnel measurements are carried out in a straight duct (with a working section of 2.4 m), a schematic of the wind tunnel is shown in figure 1. Here, we use a grid with larger mesh (M_L = 27.3 mm) on the upper half and a smaller mesh (M_S = 9.1 mm) on the lower half. Experiments are conducted at a mean velocity of 6.5 m/s. Reynolds numbers of 11,375 and 3790 correspond to M_L and M_S where the subscripts L and S indicate respectively the large and small mesh sizes. The measurements of the velocity fluctuations (u) in the longitudinal direction has been measured using a single hot-wire probe. The hot-wire (diameter $d \approx 2\mu$m; length $l = 200d$) is etched from a coil of Wollaston-Pt wire. Hot wire is operated with an ambient constant temperature anemometer (CTA) with an overheat ratio of 1.5. The output signals obtained from the CTA bridge circuit are amplified, offset and low pass filtered at a cut-off frequency (f_c) close to the Kolmogorov frequency ($f_k \equiv U_o/2\pi\eta$). Here, $\eta = \nu^{3/4} < \varepsilon >^{-1/4}$ is the Kolmogorov length scale, ν is kinematic viscosity and ε is the mean energy dissipation of turbulence. Sampling frequency (f_s) is at least

twice the f_c. For the signal digitization, a personal computer and 16 bit analogue- digital converters are used. Measurements have been made at six locations between $45M_L$ to $75M_L$, where the external flow is more homogeneous (Comte-Bellot & Corrsin, 1966). The Taylor microscale, λ, the Kolmorogov length, η and the Taylor microscale Reynolds number, R_λ, in SML are shown in table 1. Notice the relatively similar values of λ between the two grids, despite a factor 3 for the mesh ratio. On the other hand, η differs significantly between the two grids, with an average ratio, $(\eta_S/\eta_L) \simeq 1.45$. The ratio $R_{\lambda_L}/R_{\lambda_S}$ drops from about 2.3 to about 2.1 as x/M_L increases from 45 to 75. Similar ratios were reported by Veeravalli1989 for the perforated grid SML. The configuration of the grid is shown in figure 2. The solidity σ is 36% for both grids.

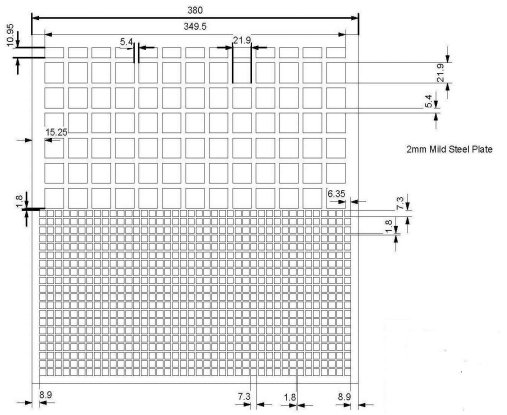

Figure 2. A schematic of the composite grid with uniform solidity used in this experimental study

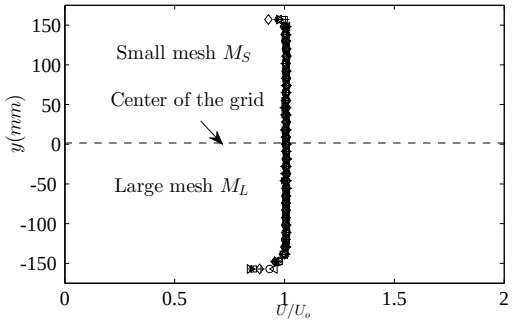

Figure 3. Mean velocity profiles at different streamwise locations, dashed line $(--)$ indicates the geometric center of the grid.

MEAN VELOCITY, TURBULENCE INTENSITY and MEAN ENERGY DISSIPATION OF TURBULENCE

Figure 3 shows mean velocity profiles at six different locations in the downstream direction of the present grid. Clearly $\frac{\partial U}{\partial y} = 0$ over a significant portion of the working section of the tunnel outside the boundary layers associated with the floor and ceiling of the section. Figure 3 also indicates that U remains constant with respect to x at all lateral positions.

The lateral distributions of the streamwise turbulence intensity at various downstream locations from the grid are shown in figure 4. At first, we note, as expected, that the turbulence intensity is decreasing in the downstream direction of the grid in both the smaller and the larger mesh regions. We also note that turbulence intensity increases as the lateral location shifts from the smaller mesh grid to the larger mesh grid, with a maximum occurring in the latter region but relatively close to the centreline. Clearly, the interaction between the two grid turbulence results in energy transfer from external quasi-homogeneous flow regions to the SML region; the larger mesh grid (larger turbulence intensity) induces a larger energy transfer than the smaller mesh grid (lower turbulence intensity). This is the first time such transfer is observed. Gilbert (1980) and Veeravalli & Warhaft (1989) measured the velocity fluctuations up to $36M$ (M = 33.5 mm corresponding to their larger mesh), while Kang & Meneveau (2008) carried out measurements in SML in an active grid turbulence in the region $x/M < 36$. However, none of them reported such energy transfer, suggesting that this transfer becomes important only at some downstream distance of the grid. Measurements are currently being carried out in the region $x/M \leq 45$ to determine the location beyond which this energy transfer becomes important. Note though that Veeravalli & Warhaft (1989) identified a mechanism that explains the energy transfer associated with the anisotropy of the flow, which gives rise to production terms in the transport equation for the Reynolds stress. Cross-wire measurements of the three velocity components will be made to investigate this mechanism.

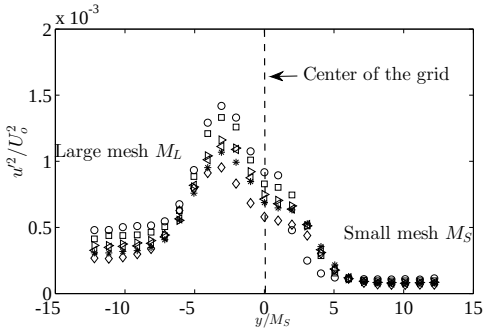

Figure 4. Comparison of the turbulence intensity profiles at different locations in the downstream direction of the grid. $x/M_L = 45(\circ)$, $x/M_L = 50(\square)$, $x/M_L = 55(\triangleleft)$, $x/M_L = 60(\triangleright)$, $x/M_L = 65(*)$, $x/M_L = 75(\diamond)$.

Figure 4 suggests that the turbulence intensity (u'^2) decreases at a faster rate for the larger mesh side than for the smaller mesh side. This is confirmed in figure 5, which shows the streamwise variation of u'^2 for both large and small mesh grids. The data are represented in log-log scales. Further, both decays appear to follow a power law, $u^2 \sim x^n$, with n being negative.

x/M_L	x/M_S	λ_L	λ_S	R_{λ_L}	R_{λ_S}	$\eta_L(mm)$	$\eta_S(mm)$
45	135	0.0050	0.0048	49.00	21.32	0.3620	0.5269
50	150	0.0054	0.0053	51.02	22.34	0.3875	0.5640
55	165	0.0056	0.0054	48.36	21.19	0.4074	0.5893
60	180	0.0059	0.0059	50.02	23.00	0.4255	0.6236
65	195	0.0060	0.0060	48.00	22.89	0.4354	0.6328
75	225	0.0065	0.0067	51.81	24.00	0.4603	0.6880

Table 1. Experimental parameters at the centre of the larger mesh and smaller mesh grid; Subscripts S and L correspond to the small and the larger meshes.

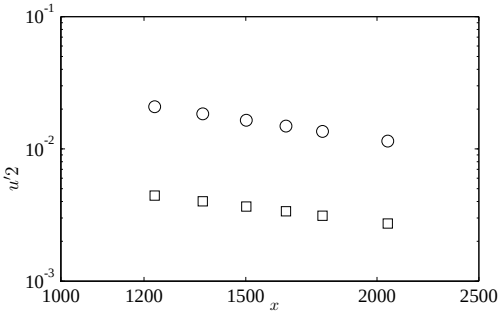

Figure 5. Decay of u'^2 downstream of the larger mesh grid, M_L (○), and smaller mesh grid, M_s (□).

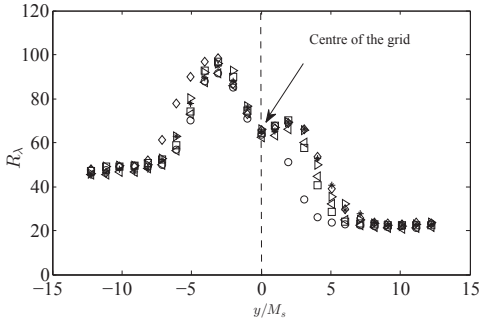

Figure 7. Lateral distributions of Reynolds number at several downstream positions

The energy production across the SML is accompanied by a increase of the mean turbulent kinetic energy dissipation ε as illustrated in figure 6, which shows its lateral distributions at several downstream locations from the grid. The isotropic form $\varepsilon_{iso} = 15\nu < (\frac{\partial u}{\partial x})^2 >$ is used as the surrogate for ε, while the Taylor hypothesis is assumed to convert the temporal derivatives to spatial derivatives. Similar to

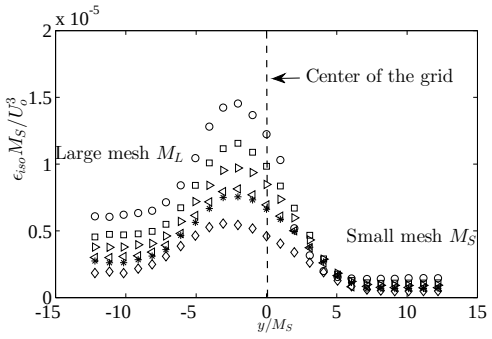

Figure 6. Comparison of the energy dissipation rates profiles at different locations in the downstream direction of the grid. $x/M_L = 45(\circ)$, $x/M_L = 50(\square)$, $x/M_L = 55(\triangleleft)$, $x/M_L = 60(\triangleright)$, $x/M_L = 65(*)$, $x/M_L = 75(\diamond)$.

the turbulence intensity, ε_{iso} decreases with increasing x/M, while it decreases faster downstream of the larger mesh grid than the smaller mesh grid.

We conclude this section by showing in figure 7 the transversal distributions of R_λ for several downstream locations. While the figure will be commented later, one can notice an interesting feature: the distributions present a double peak and they all go through a fixed point at $y/M_s = 0$, which suggests that R_λ is constant on the centreline, hinting that SP is likely to be attained.

VELOCITY STRUCTURE FUNCTIONS

Figures 8 and 9 show the distributions of the second- and the third-order velocity structure functions, $< (\delta u)^2 >$ and $< (\delta u)^3 >$, where $\delta u = (u(x+r) - u(x))$ (r is the longitudinal spatial increment obtained using the Taylor hypothesis) measured on the centreline at various downstream locations. The data are normalised by u' and λ.

Both quantities present a remarkably good collapse at all separations r. Although not show here, a similar collapse is observed when the data are normalised by the Kolmogorov scales. This indicates that both sets of scaling parameters are equivalent, which is consistent with the decay turbulence in SP. Veeravalli & Warhaft (1989) who also measured the decay of turbulence in a SML behind a perforated grid, reported that SP was not achieved in the region smaller that $x/M_L \leq 36$. Their facility prevented them to go beyond that location. This suggests that SP may not be achieved when the distance is not large enough, and would explain why Veeravalli & Warhaft (1989) could not have observed such behaviour. However, they reported that SP was achieved in the SML developing behind the bar grids. Measurements are currently being undertaken to assess whether SP can be observed or not in the region $x/M_L \leq 45$.

If collapse of $< (\delta u)^2 >$ and $< (\delta u)^3 >$ which is

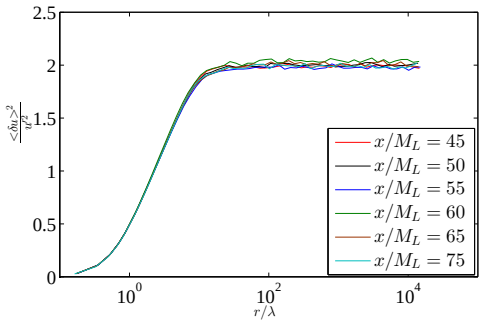

Figure 8. Second-order velocity structure function on the centreline of the grid at several downstream locations.

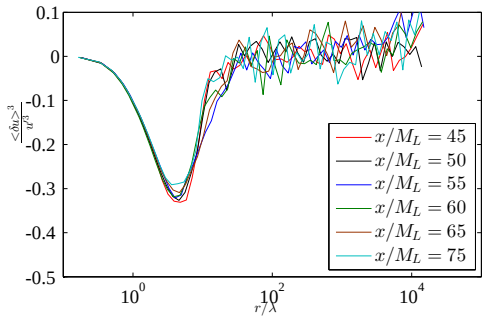

Figure 9. Third-order velocity structure function on the centreline of the grid at several downstream locations.

consistent with SP, then we can express $< (\delta u)^2 >$ and $< (\delta u)^3 >$ in their SP form:

$$< (\delta u)^2 >= u^{*2} f(r/l) \tag{1}$$

and

$$< (\delta u)^3 >= u^{*3} g(r/l), \tag{2}$$

where u^* and l are the velocity scale and the length scale (*e.g.* u' and λ, or u_K and η) functions of x only; f and g are functions of the normalised distance r/l only. If now we write the skewness of δu

$$S_r \equiv \frac{\overline{(\delta u)^3}}{[\overline{(\delta u)^2}]^{3/2}} \tag{3}$$

as

$$S_r = \frac{g(r/l)}{f(r/l)} = h(r/l), \tag{4}$$

we see that SP then implies that S_r is also a function of r/l. Thus, one expects that the distributions of S_r along the centreline to collapse onto a single curve. This is indeed observed in figure (10), which shows the centreline variations of the distribution of S_r as a function of r/η. There is an almost perfect collapse of the distributions as predicted by SP; the collapse appears less evident at small r/η, reflecting the difficulty to experimentally resolve these scales.

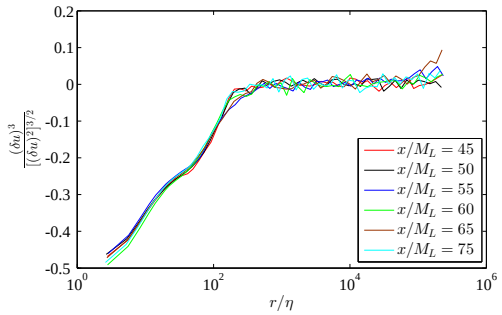

Figure 10. Profiles of S_r on the centreline of the grid at several downstream locations.

ON THE ENERGY SPECTRUM IN THE MIXING LAYER REGION

The results presented above are consistent with a SP at all scales on the centreline. To further verify that this is indeed the case, we present the one dimensional velocity spectrum along the centreline (Figures. 11 and 12, k is the wavenumber in the streamwise direction). SP at all scales should result in the collapse of the velocity spectra at all wavenumbers, regardless of the scaling length and scaling velocity used to normalise the spectra. In figures 11 and 12, the spectra are normalized by the Kolmogorov scales (η, v_K; the symbol $*$ represents Kolmorogov normalisation) and (λ, u'), respectively. There is a very good collapse at all wavenumbers when both sets of scaling variables are used. For comparison, figure 13 shows the Komogorov normalised spectra at the same streamwise location but downstream of the small mesh grid section ($y/M_s = 5$). At this off-centreline position the velocity spectra present a collapse only for $k^* \geq 1 \times 10^{-1}$ (*i.e.* small scales).

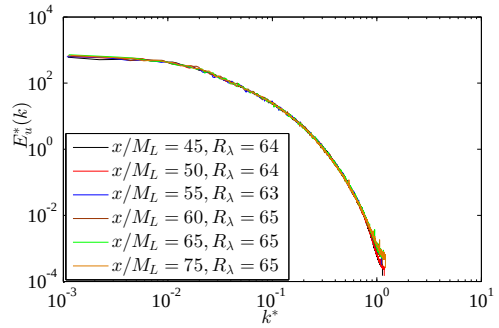

Figure 11. Kolmogorov-normalized velocity spectra at different locations along the the centreline of the grid.

The collapse of the spectra is consistent with the distributions of R_λ shown in figure 7. At the centreline R_λ appears to be constant in x while it varies at $y/M_s = 5$ as x increases. The constancy of R_λ along the centreline is well illustrated in figure 14, which presents the centreline distribution of R_λ. The reason why R_λ is constant (or equiva-

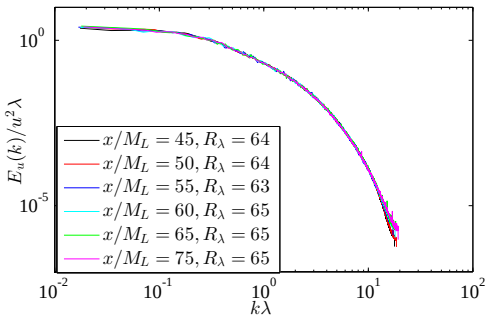

Figure 12. Taylor microscale-normalized velocity spectra at different locations along the centerline of the grid.

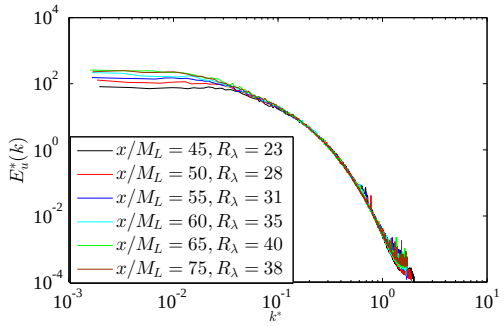

Figure 13. Energy spectrum at different R_λ in different downstream location where $y/M_s = 5$.

lently why SP is reached) on the centreline is not clear and an analysis is being currently carried out to shed some light on this issue. At this stage of the study, one can speculate that it is likely that the "transfer" of energy from the external quasi-homogeneous flow regions to the SML region (which results in a production-like energy) plays a role in the establishment of SP on the centreline. In any case, it is the first time that the SP is shown to be achieved in this particular grid turbulence, which provide an opportunity to investigate SP in a mean shearless decaying turbulence.

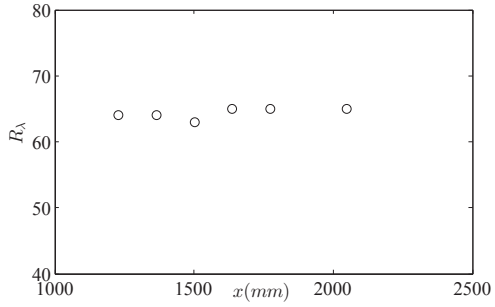

Figure 14. Distribution of R_λ along the centreline of the grid

CONCLUSION

Hot wire measurements are carried out in a SML decaying grid turbulence. The SML is generated between two grid with two different mesh sizes (mesh ratio of 3:1) but identical solidity placed side by side. It was verified that there is no mean velocity gradient across the mixing layer. As the energy decays with the distance, downstream of the composite grid, energy is transferred from the external quasi-homogeneous flow regions to the SML region. More energy is transferred from the large mesh grid than the small mesh grid. This energy transfer is consistent with a mechanism proposed by Veeravalli & Warhaft (1989), which induces production terms in the equations of the second-order and third order moments for u and v. Investigation is being carried out in the region closer to the grid ($x/M_L < 45$) to shed some light into this mechanism and its effect on the decay of turbulence. For example, it is observed that the interaction between the two grid turbulence leads to SP at all scales along the centreline of the composite grid, as illustrated by the constancy of the Taylor microscale Reynolds number and the collapse of the velocity spectra at all wavenumbers when normalised with the Kolmogorov scaling variables or the pair (u', λ).

ACKNOWLEDGEMENT

We gratefully acknowledge the financial support of the Australian Research Council.

REFERENCES

Briggs, D.A., Ferziger, J.H., Koseff, J.R. & Monismith, S.G. 1996 Entrainment in a shear-free turbulent mixing layer. *J. Fluid Mech.* **310**, 215–241.

Comte-Bellot, Genevieve & Corrsin, Stanley 1966 The use of a contraction to improve the isotropy of grid-generated turbulence. *J. Fluid Mech.* **25** (04), 657–682.

Gilbert, B. 1980 Diffusion mixing in grid turbulence without mean shear. *J. Fluid Mech.* **100** (02), 349–365.

Kang, H. S. & Meneveau, C. 2008 Experimental study of an active grid-generated shearless mixing layer and comparisons with large-eddy simulation. *Phy. Fluids (1994-present)* **20** (12), 125102.

Knaepen, B.and Debliquy, O. & Carati, D. 2004 Direct numerical simulation and large-eddy simulation of a shear-free mixing layer. *J. Fluid Mech.* **514**, 153–172.

Tordella, D. & Iovieno, M. 2006 Numerical experiments on the intermediate asymptotics of shear-free turbulent transport and diffusion. *J. Fluid Mech.* **54954**, 429–441.

Veeravalli, S. & Warhaft, Z. 1989 The shearless turbulence mixing layer. *J. Fluid Mech.* **207**, 191–229.